

Idealization of pericellular fluid space geometry and dimension results in a profound underprediction of nano-microscale stresses imparted by fluid drag on osteocytes

Eric J. Anderson^a, Melissa L. Knothe Tate^{a,b,*}

^aDepartment of Mechanical and Aerospace Engineering, Case Western Reserve University, Cleveland, OH 44106, USA

^bDepartment of Biomedical Engineering, Case Western Reserve University, 10900 Euclid Avenue, Cleveland, OH 44106, USA

Accepted 27 February 2008

Abstract

To date, no published study has examined quantitatively the effect of geometric and dimensional idealization on prediction of the mechanical signals imparted by fluid drag to cell surfaces. We hypothesize that this idealization affects the magnitude and range of imparted forces predicted to occur at a subcellular level. Hence, we used computational fluid dynamics to predict magnitudes and spatial variation of fluid velocity and pressure, as well as shear stress, on the cell surface in two- and three-dimensional models of actual and idealized pericellular canaliculi geometries. Furthermore, variation in actual pericellular space dimensions was analyzed statistically based on high-resolution transmitted electron micrographs (TEM). Accounting for the naturally occurring protrusions of the pericellular space delineating *lamina limitans* resulted in predictions of localized stress spikes on the cell surface, up to five times those predicted using idealized geometries. Predictions accounting for actual pericellular geometries approached those required to trigger cell activity in *in vitro* models. Furthermore, statistical analysis of TEM-based dimensions showed significant variation in the width of the canaliculi space as well as the diameter of the cell process, both of which decrease with increasing distance from the cell body. For the first time to our knowledge, this study shows the influence of physiologic geometry *per se* on the nano-scale flow regimes in bone, and the profound influence of physiologic geometry on force magnitudes and variations imparted locally to cells through load-induced fluid flow.

© 2008 Elsevier Ltd. All rights reserved.

Keywords: Stress/strain; Cell mechanics; Mechanical loading; Osteocytes; Mechanotransduction

1. Introduction

The fluid milieu of osteocytes provides a means for transfer of both mechanical and biochemical signals via fluid flow and associated convective transport (Pienkowski and Pollack, 1983; Frost, 1987; Reich and Frangos, 1991; Knothe Tate et al., 1998a, b; You et al., 2001; Knothe Tate, 2001a, b, 2003). Interestingly, the load magnitudes required to elicit changes in cell activity *in vitro* are an order of magnitude higher than loads shown to elicit bone adapta-

tion *in vivo* (Rubin and Lanyon, 1984; Almekinders et al., 1993; Weinbaum et al., 1994; Guilak et al., 1995; Klein-Nulend et al., 1995; Owan et al., 1997; Smalt et al., 1997; Jacobs et al., 1998; Fritton et al., 2000; You et al., 2000; Donahue et al., 2003; Han et al., 2004; Anderson et al., 2005; McGarry et al., 2005; Nicolella et al., 2006; Anderson and Knothe Tate, 2007) (Table 1). The impetus for this study was to determine potential sources for the order of magnitude discrepancy in loads required *in vivo* and *in vitro* to trigger bone adaptation by cellular remodeling.

Predictive computer models allow determination of parameters that most influence the mechanical environment of the cell (Han et al., 2004; Steck and Knothe Tate, 2005; Anderson et al., 2005, 2006) but pericellular

*Corresponding author at: Department of Biomedical Engineering, Case Western Reserve University, 10900 Euclid Avenue, Olin 219, Cleveland, OH 44106, USA. Tel.: +1 216 368 5884; fax: +1 216 368 4969.
E-mail address: knothetate@case.edu (M.L. Knothe Tate).

Table 1

Range of predicted stress magnitude from *in vivo* studies are up to an order of magnitude lower than stresses required to elicit cellular activity above baseline *in vitro* cell studies

| | |
|-------------------------|-------------------------------|
| <i>In vivo</i> models | Goodship et al. (1979) |
| 0.5–2 Pa | Rubin and Lanyon (1984) |
| <0.2% microstrain | Fritton et al. (2000) |
| <i>In vitro</i> studies | Reich and Frangos (1991) |
| 3–5 Pa | Almekinders et al. (1993) |
| >2% microstrain | Burger and Veldhuijzen (1993) |
| | Guilak et al. (1995) |
| | Klein-Nulend et al. (1995) |
| | Owan et al. (1997) |
| | Smalt et al. (1997) |
| | You et al. (2000) |
| | McGarry et al. (2005) |
| | Nicolella et al. (2006) |

geometries are typically idealized for computational efficiency (Anderson et al., 2005; Han et al., 2004; Weinbaum et al., 1994). Osteocytes are surrounded by a fluid-imbibed extracellular matrix whose resistance to fluid flow increases with increasing degree of mineralization; the *lamina limitans* refers to the layer of pericellular matrix (PCM) closest to the cell process, whose outer edge is defined by the mineralization front and, hence, delineates the wall of the canaliculus (Scherft, 1972). Yet, the surface roughness and naturally occurring protrusions of the *lamina limitans*, are typically neglected in idealized models (Knothe Tate and Neider, 1998; Knothe Tate, 2001b).

To date, no published study has examined quantitatively the effect of geometric and dimensional idealization on prediction of the mechanical signals imparted by fluid drag to cell surfaces. We hypothesize that this idealization affects the magnitude and range of imparted forces predicted to occur at a subcellular level. In this study, we implement geometries obtained from actual high-resolution electron micrographs of pericellular fluid spaces (canaliculi). Computational fluid dynamics is used to calculate flow in the pericellular space under physiologic loading conditions. Parametric studies are then carried out to elucidate the effect of wall protrusions on model predictions. In an additional case study, a microcrack is added virtually to the physiologic geometry to investigate the effect of microdamage on predictions of fluid behavior. Finally, a statistical analysis of the micrograph geometries is also performed to investigate variation in the pericellular fluid space dimensions and to place computational model predictions in the context of naturally occurring micro-anatomical variations. For this purpose, measurements of the annular fluid space in the canaliculus as well as the cell-process diameter are taken from high-resolution micrographs; variation and dimension of pericellular fluid spaces are determined as a function of location with respect to the cell body.

2. Methods

Actual geometries of pericellular spaces were obtained from digitized transmitted electron micrographs (TEM) prepared during the course of a previous study (see Knothe Tate et al., 1998a; Reilly et al., 2001; Knapp et al., 2002). Animals were injected *in vivo* with horseradish peroxidase or microperoxidase to mark the outer edge of the pericellular fluid space, referred to as the *lamina limitans*. Specimens were obtained from the femoral diaphyses of three skeletally mature, age and gender-matched rats. TEM images were acquired at five magnifications and sorted to obtain a subset of 16 images that included detailed geometry of pericellular channels.

Measurements were carried out and recorded electronically using imaging software (OpenLab 4.0.3) to characterize the variation in pericellular flow space geometries, including cell process and canalicular diameters and their variations as a function of their distance from the cell body. The annular fluid space dimensions, from the outer edge of the space (canalicular wall) to the surface of the cell process, were recorded and measured at 0.1 μm intervals where possible. In the 16 images studied, parameters were recorded as a function of animal number, treatment with microperoxidase, horseradish peroxidase and a physiological saline control, and image magnification. Measurements were exported for analysis of variance (ANOVA) testing to determine: (1) variance of the annular-gap size in the pericellular network as a function of animal, peroxidase type, and magnitude; (2) variance in process diameter as a function of animal, peroxidase type, and magnitude; (3) variance of annular-gap size with process diameter and (4) process diameter and annular-gap size as a function of distance from the cell body. A simplified one-way ANOVA test was performed to determine the influence of each factor; interactions between factors (animal, peroxidase type, magnification) were assumed to be negligible both from technical as well as biological perspectives.

The image showing best resolution of unmineralized fluid space geometry, defined as the longest continuous canalicular channel with complete cell process and *lamina limitans*, was exported for predictive flow studies, which were carried out using a dimensionless analysis of the Navier–Stokes equations (described later in the text). A section of the pericellular fluid space showing the natural geometric complexity at high resolution (micro- and nano-scales) was chosen to model the actual microanatomic geometry of the periosteocytic flow channel in two and quasi-three dimensions. By starting with an area representative of highest geometric complexity and iteratively idealizing the geometry, the effect of actual geometric complexity and iterative idealization of geometry on periosteocytic flow predictions could be assessed (Fig. 1A).

Progressive idealization was applied iteratively, from the representative microanatomic geometry to a highly idealized straight tube model (Fig. 1B, i–iv), to create flow geometries that were subsequently meshed into nodes for numerical simulation of flow through the space (which is achieved through numerical analysis of the Navier–Stokes equations at each node in the mesh). The first case study (i) includes the protrusions of the mineralized matrix into the unmineralized pericellular fluid space. A nodal mesh of that space is created by tracing the representative micrograph geometry. In a second case study (ii) idealization is introduced through smoothing the rough canalicular boundary by fitting a polynomial function to a series of points taken along the actual pericellular fluid space geometry, thereby creating an idealized, “smoothed” wall profile from representative anatomical points. In a third case study (iii) the wall profile is further idealized (and smoothed) by fitting an arc function to three points comprising the inlet, midpoint and outlet of the anatomical flow channel. Finally, the most idealized case (iv) is created as a straight annular channel, representing the pericellular flow space defined between the surfaces of the mineralized matrix and the osteocyte process. For the most idealized model of flow through a straight annular channel, the flow channel dimensions were varied based on physiological dimensions, from 0.01 to 0.2 μm , to achieve estimated ranges in predicted forces imparted by the fluid on the process surface. Nodal meshes for each model variation comprise a structured grid and are adapted systematically until solutions are found to be grid independent. For the four cases studied

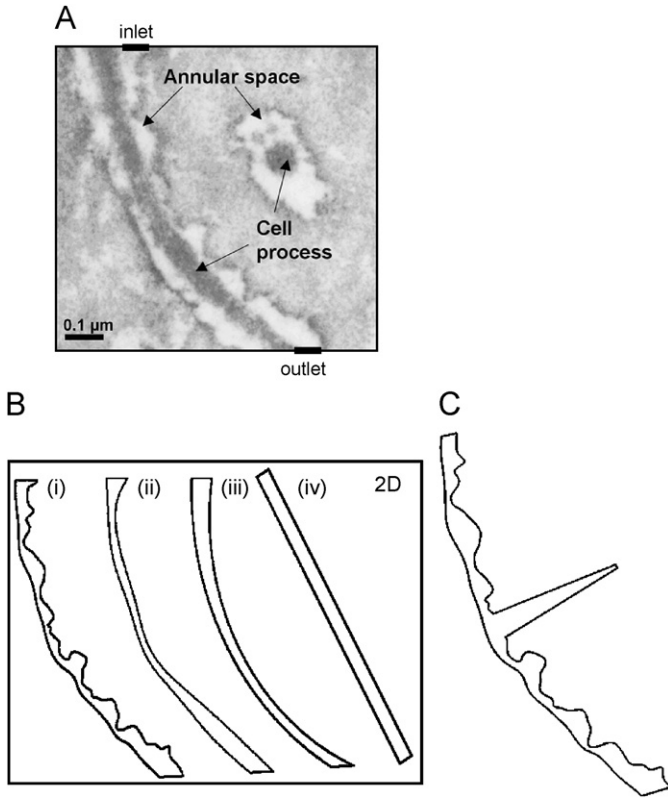


Fig. 1. (A) TEM image of canaliculus, including cell-process and surrounding matrix microporosity, from a rat that received intravital injection of microperoxidase tracer. The precipitate produced by the reaction of the peroxidase with diaminobenzidine (dark areas at edges) marks the outer edge of the pericellular fluid space, also referred to as the *lamina limitans*. The fluid space is likely filled with a proteoglycan network and resistance to flow within this space is much less than resistance to flow through the extracellular matrix (gray area beyond the dark edges). (B) Geometries implemented to study how progressive idealization of the pericellular fluid space geometry influences predictions of shear stress imparted to osteocytes. One half of the two-dimensional fluid space around the cell process is depicted, bounded by the cell process on the left and *lamina limitans* on the right. The space is iteratively idealized, from: (i) an actual wall tracing including micro-nanoanatomical geometry, (ii) a wall idealized by fitting a polynomial function to multiple points from the actual geometry, (iii) a wall idealized by fitting an arc-function to three points from the actual geometry, to (iv) a most highly idealized straight annular channel approximating the actual geometry. (C) Anatomically based model including a microcrack. The crack acts as a discontinuity in the flow area.

(Fig. 1B, i–iv), the number of nodes are 18557, 4776, 1976, and 171, respectively.

Additional models are used to determine effects of geometrical variations in three dimensions. Since current imaging capabilities do not allow for high-resolution three-dimensional imaging of subcellular fluid space geometry, the two-dimensional representative anatomical wall profile is revolved about the axis of the cell process (axisymmetric) best approximate the three-dimensional geometry (Fig. 2). To investigate the effects of non-axisymmetric, protruding discontinuities on flow in three dimensions, a second annular model is created. In addition, to account for the effect of an extruding discontinuity (expands the flow geometry into the plane of the matrix) on flow, e.g. created by a microcrack extending the fluid space into the plane of the matrix, another case study is carried out with an anatomical wall profile that is extended into the plane of the

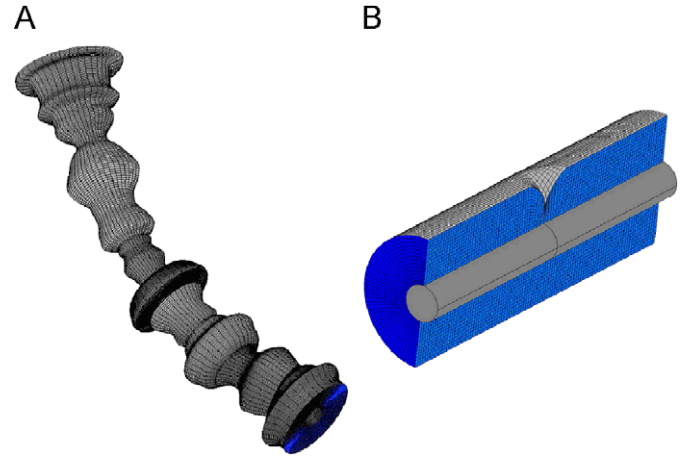


Fig. 2. Three-dimensional models of the pericellular volume: (A) axisymmetric geometry, created by revolving the representative two-dimensional anatomical wall profile about the axis of the cell process, (B) non-axisymmetric geometry containing a single protrusion point in a highly idealized annular fluid space.

matrix by a microcrack. The microcrack's width is on the order of magnitude of the annual gap width between the surface of the cell process and the mineralized matrix, based on dimensions from a previous study (Tami et al., 2002) (Fig. 1C). When the microcrack is included in the model geometry, the process length is identical to the previous cases; however, the relative placement of the mineralized matrix and protrusions are shifted due to the insertion of the microcrack.

In all cases, pericellular flow is calculated numerically at each node in the fluid mesh, using a second-order finite-volume method (CFD-ACE, Huntsville, AL), where continuity (1) and low-Reynolds number ($Re \ll 1$) Navier–Stokes equations (2) were solved in two dimensions for each case study:

$$\nabla \cdot V = 0 \quad (1)$$

$$0 = -\nabla P + \mu \nabla^2 V \quad (2)$$

where V is the velocity vector, P is local fluid pressure, and μ is viscosity. Pressure gradients at the level of the canaliculus oscillate and encompass a range of values (Anderson et al., 2005); hence, dimensionless variables are used to describe pressure, velocity, and shear stress, yielding a general solution that can be scaled up or down to apply for any physiologic load magnitude and/or fluid geometry dimension. Defining the following dimensionless variables and substituting into (1,2), scales for pressure, velocity and shear stress are found for a given pressure at the inlet (assuming outlet pressure is set to zero),

$$P^* = \frac{P}{P}, \quad u^* = \frac{u}{U}, \quad x^* = \frac{x}{L}, \quad y^* = \frac{y}{D}, \quad v^* = \frac{vL}{UD}$$

$$0 = -\frac{P}{L} \frac{\partial P^*}{\partial x^*} + \mu \frac{U}{L^2} \left[\frac{\partial^2 u^*}{\partial x^{*2}} + \frac{L^2}{D^2} \frac{\partial^2 u^*}{\partial y^{*2}} \right]$$

$$0 = -\frac{P}{D} \frac{\partial P^*}{\partial y^*} + \mu \frac{UD}{L} \left[\frac{1}{L^2} \frac{\partial^2 v^*}{\partial x^{*2}} + \frac{1}{D^2} \frac{\partial^2 v^*}{\partial y^{*2}} \right]$$

$$U = \frac{PD^2}{\mu L}, \quad \frac{\partial P^*}{\partial y^*} = 0$$

$$u^* = \frac{\mu L}{PD^2} u, \quad v^* = \frac{\mu L^2}{PD^3} v, \quad P^* = \frac{P}{P}, \quad \tau^* = \frac{\tau}{P} \left(\frac{L}{D} \right)$$

where u is axial velocity, v is transverse velocity, x is axial dimension, y is transverse dimension, U is maximum transverse velocity, $L = 1.3 \mu\text{m}$ is axial length of model (taken from image), $D = 0.082 \mu\text{m}$ is inlet height of model, P is applied inlet pressure, τ is wall shear stress on cell process.

Using pressure-induced flow, boundary conditions at the inlet and outlet for dimensionless pressure are given as 1 and 0, respectively, and the no-slip velocity condition is applied at the canalicular and process walls. The fluid medium is assumed to be similar to 0.9% saline (slightly more viscous than water) at 310 K ($\mu = 0.001$ kg/ms), although the viscosity affects only the dimensionless velocities, not the wall shear stress (see scales above). All structures are considered to be rigid or non-deforming to focus on changes in flow regimes due to naturally occurring variations in anatomic geometries. The unmineralized space between the surface of the cell process and the mineralized bone matrix was treated as homogeneous, because the resistance to flow within this space is taken as orders of magnitude less than flow through the mineralized matrix (Knothe Tate, 2003; Anderson et al., 2008). A parametric study was carried out to test this assumption. Finally, conservation of mass and momentum are satisfied as solutions are found to converge to a criterion of 0.00001 in each case.

3. Results

Idealizations of pericellular flow channel geometries exert a profound influence on fluid flow predictions. In the two-dimensional models created from TEM micrographs, progressive idealization, from anatomic wall profiles to straight pipe flow, results in progressive underestimates of flow magnitudes and shear stresses imparted by fluid drag over cell membranes. Furthermore, simplifying pericellular geometry from a physiologic to highly idealized state yields a reduction in both the range and magnitude of shear stress imparted to the surface of the cell process.

In the case study with fluid space defined by the representative anatomic wall profile, matrix protrusions in the pericellular space cause sharp local spikes in axial velocity (Fig. 3A and B) and shear stresses imparted at the cell surface. For the representative anatomic geometry studied, seven spikes in stress are observed, reaching a maximum value of 0.58.

In the first step of idealization, smoothing of the canalicular wall via a polynomial function results in a reduction in both the magnitude as well as in the variance of shear stress along the cell process compared to the anatomic case (Fig. 3C and D). Here, the smoothed wall retains two elongated protrusions, where local velocity and stress increase as well. Furthermore, the idealization process effectively increases the gap between the cell surface and mineralized matrix (*lamina limitans*), causing a reduction of maximal shear stress on the surface of the cell process, from 0.58 (anatomic) to 0.39 (smoothed).

In second iterative step of idealization an arc function is fit to the inlet, central and outlet points of the anatomic wall profile. This idealization results in complete smoothing of anatomic matrix protrusions and, hence, elimination of spikes in shear stress along the cell surface (Fig. 3E and F). Similar to the polynomial idealization process, the arc function fitting effectively decreases the gap between the surface of the cell process and the canalicular wall, resulting in a relative increase in fluid velocity, peaking at a distance 0.8 times the total process length. The

corresponding wall shear stress at this point is 0.4, which is less than the 0.58 peak wall stress reached in the anatomical wall profile case. Hence, although the magnitude of the peak stress is similar to the case with polynomial curve idealization, the variation in stress along the length of the process is further reduced.

In the most idealized case, where the anatomic flow profile is idealized as a straight annular channel, the velocity profile is constant along the cell process. Although constant, fluid velocity magnitudes as well as magnitudes of shear stresses (imparted on the cell process by flow) depend on the definition of the fluid channel width (Fig. 6A and B). By using a range of gap sizes, 0.01–0.2 μm , taken from measurements within the images, nondimensionalized shear stresses are predicted numerically to be between 0.1 and 1.2, respectively.

Accounting for the third dimension, flow prediction trends are reiterated, but additional effects are observed. In an axisymmetric three-dimensional model created by revolving the anatomic wall profile about the axis of the cell process, the added dimension amplifies the magnitudes of fluid velocity and shear stress along the cell process. Comparing results in analogous planes from the two- and three-dimensional studies, the axial velocity distribution is similar for both cases, but the spikes in flow and shear stress are higher in the 3D case compared to the 2D case (Fig. 4A). Consequently, the shear stress imparted to the cell process wall is similar, where three-dimensional variance along the surface is found (Fig. 4B). Comparing profiles of wall shear stress in the two- and three-dimensional models, the added dimension amplifies the imparted stress up to twofold (Fig. 4C). Here, the magnitude of the maximum stress spike increases from 0.58 to 0.77 for the axisymmetric anatomic geometry.

Contrary to axisymmetric models, interstitial fluid moves around the single protrusion point in the non-axisymmetric model including a single protrusion. Following the path of least resistance, the fluid diverges near the matrix protrusion, where the axial velocity beneath the protrusion decreases, while the transverse and radial velocities increase due to continuity (Fig. 5A–D). Nonetheless, with the reduced gap size at the protrusion location, the derivative of velocity still increases at this point, and thus, the shear stress on the process wall spikes directly below the protrusion point (Fig. 5E and F). Interestingly, shear stress on the process surface is also found to decrease immediately before the protrusion, thus adding to the relative increase in magnitude at the stress spike.

Finally, when a discontinuity representing a microcrack is included in the anatomic model, the axial velocity decreases at the location of the crack (Fig. 6C and D). As a result, the shear stress on the process surface decreases at the corresponding location. However, due to shifting of the mineralized matrix and protrusions, the stress profile along the cell surface is shifted as well. In general, spikes in shear stress are dampened near the microcrack with the

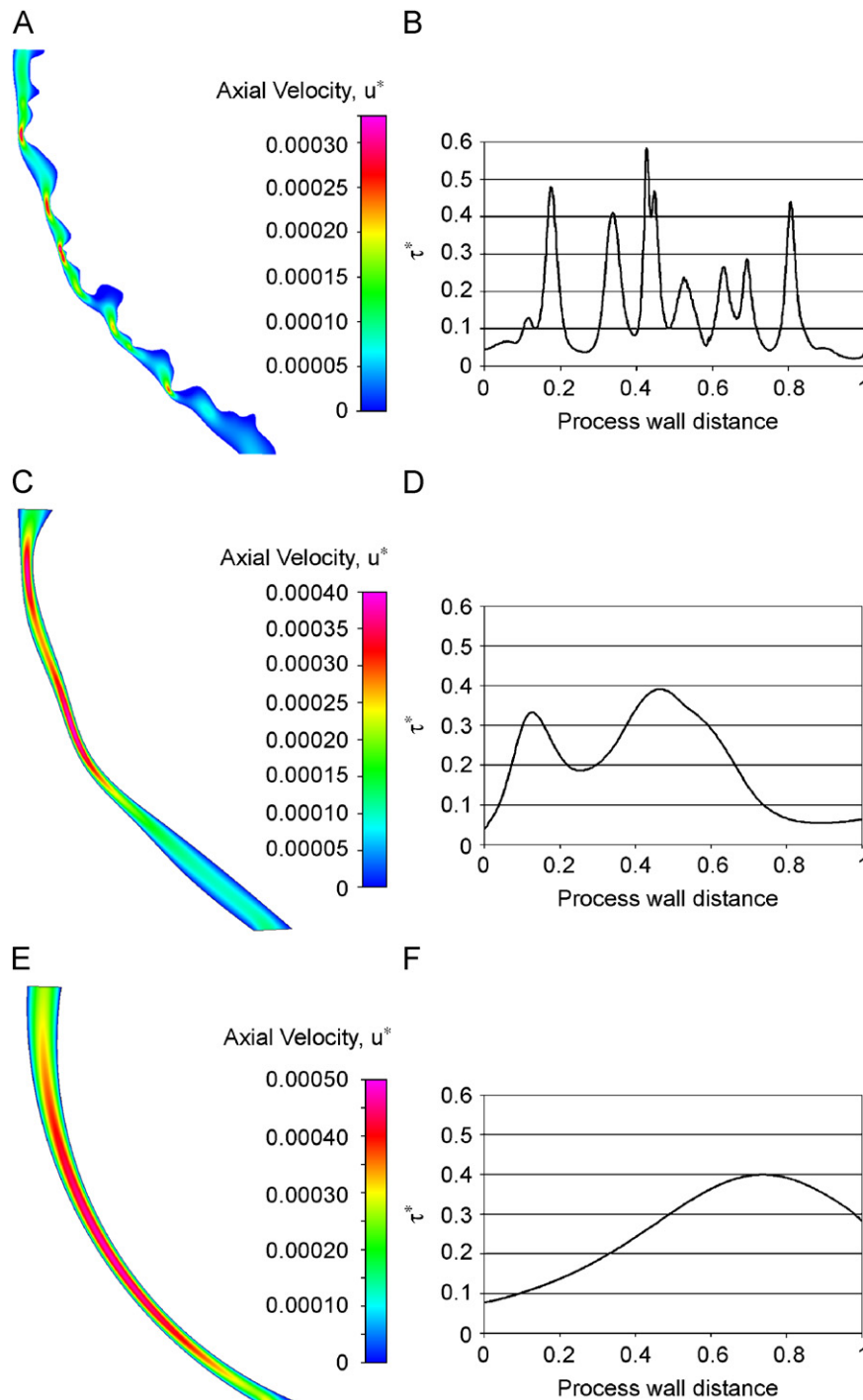


Fig. 3. Non-dimensionalized (left) axial velocity, and (right) shear stress on the surface of the cell process, from inlet (0) to outlet (1, top to bottom in axial velocity plot). Case study (A,B) with anatomic geometry containing wall protrusions, (C,D) in which the anatomic wall profile is smoothed using a polynomial function, (E,F) in which arc geometry is created from 3 points.

reduction in velocity, where in areas away from the microcrack, the stress can potentially increase or decrease depending on the specific shift of the geometry. In this case, the canalicular wall geometry is shifted along the axis of the canaliculus to create the microcrack, causing an amplification of shear stress as compared to the physiologic model, with spikes up to 0.08 (Fig. 6).

Finally, statistical analysis of the TEM images shows that both the width of the pericellular space between the process wall and the mineralized matrix as well as the cell-process diameter are highly variable, as observed in the representative anatomic geometry implemented for predictive flow studies. The pericellular space exhibits a mean gap size of $0.131 \mu\text{m}$ ($\pm 0.056 \mu\text{m}$, $n = 16$). The mean

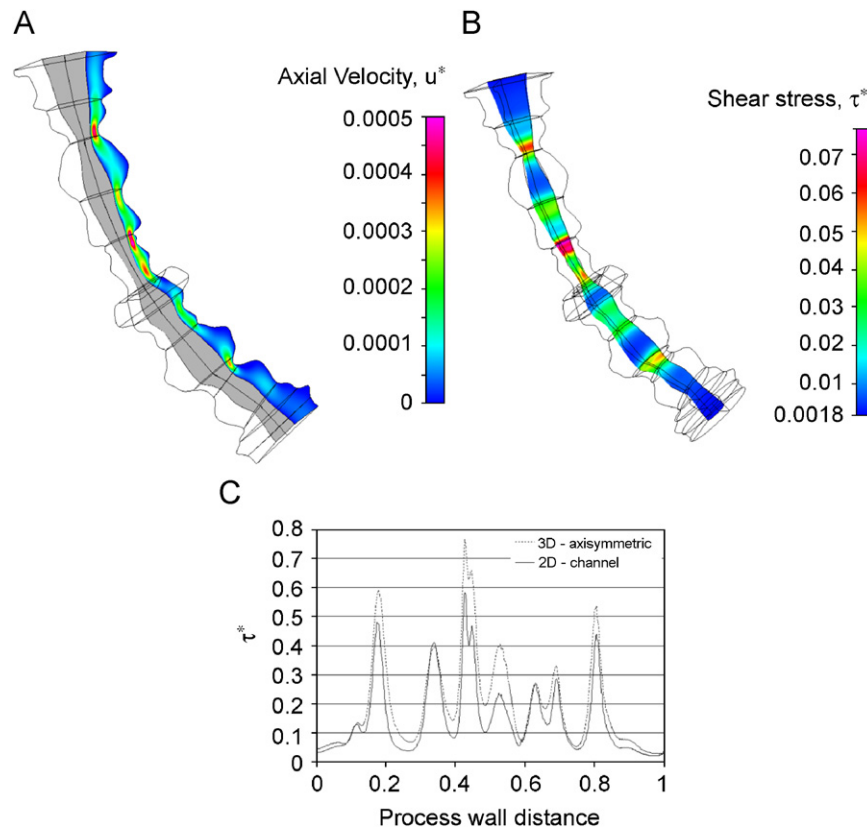


Fig. 4. Axisymmetric model created by revolving the anatomic wall profile about the axis of the cell process: non-dimensionalized plots of (A) axial fluid velocity, (B) shear stress imparted by the fluid on the surface of the cell process, and (C) a plot comparing the shear stresses along the surface of the cell process, predicted for the two- and three-dimensional cases.

cell-process diameter is $0.099\ \mu\text{m}$ ($\pm 0.029\ \mu\text{m}$ standard deviation). ANOVA testing shows that the pericellular fluid space dimensions (as well as process diameter) are independent of animal (p -value = 0.492), and peroxidase type (p -value = 0.425). As animal and peroxidase type were found to have no effect on gap size and process diameter, magnification could be investigated without holding these factors constant. In this test, magnification is found to be significant (p -value < 0.0001). Comparing confidence intervals for each magnification group, it is found that the measured gap size differs significantly between groups 1 and 2 only, and thus inferences on gap size and process diameter were made within a magnification level for the following regression analysis.

Looking at the variation in gap size and process diameter at the highest magnification, the width of the pericellular fluid space tends to increase with cell-process diameter, but no significant correlation can be made ($R^2 = 59\%$, Fig. 7A); from qualitative observations, the gap size is highly variable along the length of the process due to the presence of matrix protrusions into the fluid space. Also, there is a significant correlation between the diameter of the cell process and the distance from the cell body at which the measurement is made, where the cell-process diameter decreases with increasing distance from the cell body ($R^2 = 78\%$). Pericellular fluid gap dimensions also

decrease with distance from the cell body, but no statistically significant correlation between the two shows ($R^2 = 55\%$, Fig. 7B and C).

4. Discussion

Idealization or simplification of pericellular fluid space geometry and dimension results in a profound underprediction of nano-microscale stresses imparted by fluid drag on osteocytes. Implementation of actual physiological geometries at the cell and sub-cell scales increases the magnitude of shear stresses at the surface of the cell process by fivefold (eightfold in three-dimensional models), bringing predicted stresses into the range of those reported experimentally *in vitro* to trigger a change in baseline cell activity. The underestimation of physical parameters due to progressive idealization of the physiologically complex pericellular fluid space geometry includes underestimation of fluid pressures, flow velocities, as well as the previously mentioned shear stresses imparted by flow at interfaces between the fluid and cells. Hence, this computational study provides data supporting the postulate that physiological encroachments of the mineralized matrix wall into the fluid space (Knothe Tate, 2001a; Reilly et al., 2001) influence flow fields and resultant shear stresses on the cell surface. Furthermore, accounting for local spikes in shear

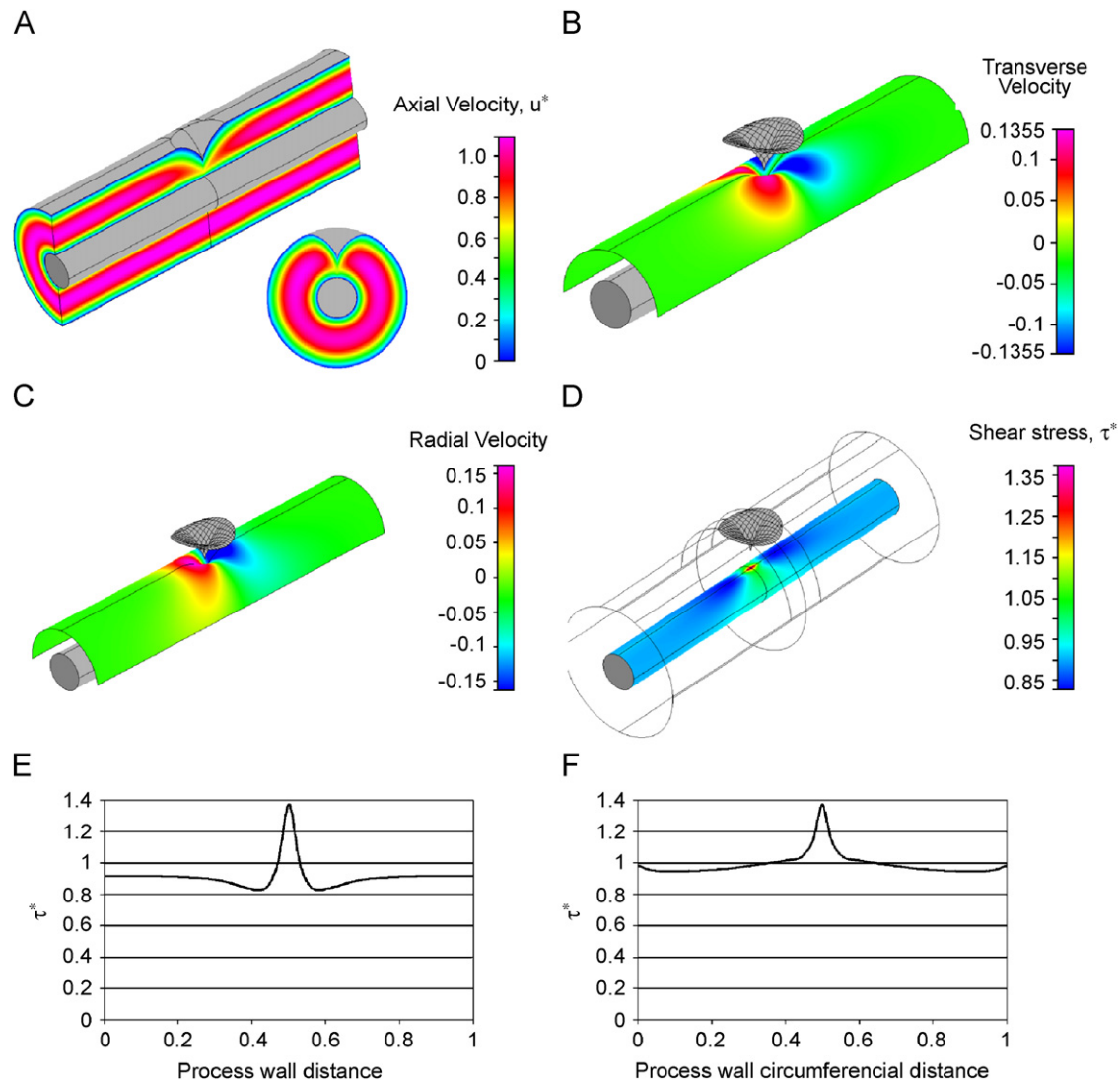


Fig. 5. Three-dimensional model including a singular protrusion, to account for effects not included in the axisymmetric model: non-dimensionalized plots of (A) axial fluid velocity, (B) transverse fluid velocity, and (C) radial fluid velocity, all of which are scaled with a maximum velocity of 3.28×10^{-5} m/s, as well as (D) shear stress imparted by fluid drag on the process wall. Shear stress on the surface of the cell process, and (E) along the length of the cell process from inlet (0) to outlet (1) and (F) circumferential distance located at the protrusion point.

stress as well as average shear stresses reported in other *in silico* models (Anderson et al., 2005), local shear stresses occurring due to physiological loading are likely much higher than those previously predicted to occur. Local *in vivo* shear stresses may even approach those required to trigger cell activity in *in vitro* models (Knothe Tate, 2001b). For the first time to our knowledge, this study shows the influence of physiologic geometry *per se* on the nano-scale flow regimes in bone, and the profound influence of physiologic geometry on force magnitudes and variations imparted locally to cells through load-induced fluid flow.

In the two-dimensional and three-dimensional axisymmetric models, both velocity and stress on the process wall increase dramatically at each protrusion point. Velocity and shear stress imparted at the cell surface are similar but

amplified in the axisymmetric (3D) model. In the non-axisymmetric 3D model, however, flow diverges around the protrusion point, which decreases the velocity magnitude but increases its derivative; the increase in the derivative of velocity results in an increase in shear stress imparted by fluid drag on the cell surface at the location of the protrusion. Thus, the 3D models validate the results of the 2D models and provide further evidence of stress amplitude spikes at sites where the *lamina limitans* encroaches into the pericellular fluid space. These 2D and 3D case studies provide compelling evidence for “stress amplification” intrinsic to the fluid canal geometry; future cell biological studies will elucidate whether subcellular structures such as hemidesmosomes co-localize with sites of “stress amplification”, providing an efficient means to harness mechanical signals for transduction to the nucleus.

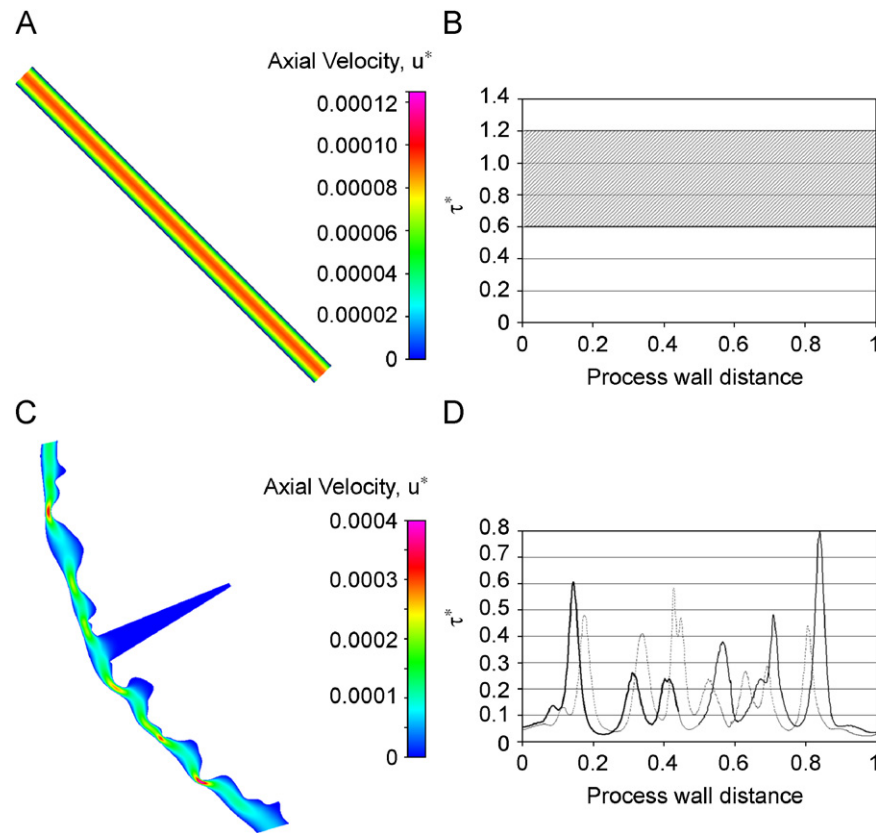


Fig. 6. (A,B) Most highly idealized model, where the anatomic flow profile is idealized as a straight, annular pipe: plots of non-dimensionalized axial velocity (left) show constant flow velocity distributions along the length of the process, corresponding to constant shear stress (right) imparted on the cell process surface, from inlet (0) to outlet (1) for non-dimensionalized pericellular gap spacing from 0.3–0.6. Of note, stresses remain constant across the surface, in contrast to stress spikes and stress variations predicted for the anatomic profile geometry and previous idealizations. (C,D) Addition of a microcrack to the model with anatomic wall profile: non-dimensionalized plots of (left) axial velocity, and (right) shear stress on the surface of the cell process (black), compared to shear stresses on the surface of the cell process where no microcrack is present (gray). Spikes in shear stress are dampened near the microcrack and amplified in areas away from the microcrack.

Geometric idealization results in predicted shear stresses that may overlap with average values of physiological stresses, but that lack the local maxima and variance observed in predictions based on actual physiologic geometries. The loss of peak stresses and natural variation in stresses associated with geometrical idealization can be attributed directly to the elimination of local encroachments of the *lamina limitans* into the pericellular fluid cavity. Statistical analysis of high-resolution subcellular scale images show that the mean width of the pericellular space between the process wall and mineralized matrix (*lamina limitans*) is similar to that reported in the literature (0.131 μm) but that the gap size is highly variable due to the complex geometry and encroachment of the *lamina limitans*, thus underscoring the importance of natural anatomic variation in pericellular geometry and dimension when predicting flow regimes at the subcellular scale. In addition, the pericellular gap size, as well as the cell-process diameter, decrease with increasing distance from the cell body; both the pericellular gap size and the cell-process diameter taper off as they approach the gap junction.

The case study including a microcrack to investigate the effect of damage on mechanical signal transduction showed that naturally occurring local spikes in shear stress are dampened near the microcrack and amplified up to 1.5-fold in areas away from the microcrack (compared to the same geometry without a microcrack). Recent work has implicated microdamage as a potent stimulator of remodeling and bone turnover (Tami et al., 2002; Verborgt et al., 2000). The data presented here indicate that cell level stresses may provide a means to detect and respond to changes in local stresses near microcracks; thus, changes in mechanical signals due to the presence of microdamage may not only trigger processes associated with cellular remodeling but also could provide a means for osteoclasts to locate damaged sites.

Limitations in this study arise from current inherent constraints in obtaining high-resolution images of pericellular fluid space geometries. Currently, it is not possible to obtain a three-dimensional image of both cellular and matrix geometry at a sub-cell scale resolution without the introduction of artifacts. We addressed this limitation by using a combination of models based on actual

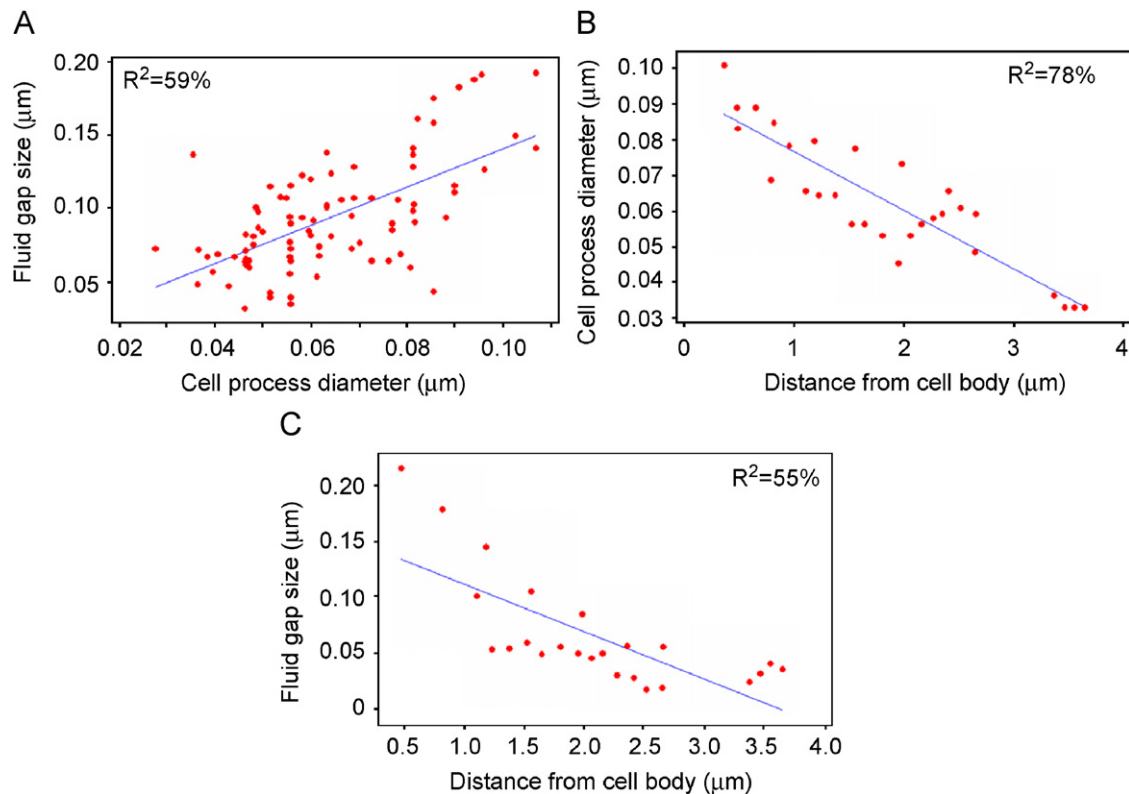


Fig. 7. Statistical analysis of dimensions measured on TEM images: (A) fluid gap size as a function of cell-process diameter ($R^2 = 59\%$), (B) cell-process diameter as a function of distance from the cell body ($R^2 = 78\%$), and (C) fluid gap size as a function of distance from the cell body ($R^2 = 55\%$).

two-dimensional geometries as well as approximated three-dimensional geometries. Similarly, the effect of geometrical changes due to the presence of a microcrack were approximated due to limitations in subcellular resolution imaging of bone microdamage. In addition, although we used protocols to best maintain the geometry of the cell process and *lamina limitans* during histological processing and used state of the art tracer and imaging techniques, the ultrastructure of the PCM cannot be visualized at this length scale. Thus, the ultrastructural geometry of the pericellular space is not included explicitly in the model and is accounted for by defining parameters such as porosity and permeability of the PCM obtained from the literature (Weinbaum et al., 1994; Han et al., 2004; You et al., 2004; Anderson et al., 2008), where the influence of the matrix protrusions were present regardless of these parameters. Furthermore, this study addresses fluid forces imparted by fluid drag at the surface of the cell process and not the solid mechanics (dynamics) associated with cellular structures. The surface of the cell process is likely much more compliant than that of the *lamina limitans* and will hence deform more under flow-induced drag, which will affect the magnitude of the shear stress at the interface. Ongoing modeling includes compliant cell structures such as the cytoskeleton, cell membrane, transmembrane proteins and the cytosol.

In conclusion, idealization of pericellular fluid space geometry causes a profound underestimation of forces transduced to the cell from load-induced fluid flow, potentially accounting for the several orders of magnitude discrepancy in *in vivo* and *in vitro* predictions of cell behavior in response to flow. Not only do such idealizations alter predictions of the cell's mechanical environment, but also local shear stresses on the cell process are likely to be higher and more variable than previously predicted. Inclusion of more physiologic geometries in computational models results in predictions of peak shear stresses on the cell process that approach magnitudes shown to trigger cell activity in *in vitro* models (Burger and Veldhuijzen, 1993; Klein-Nulend et al., 1995; Almekinders et al., 1993; Guilak et al., 1995; Owan et al., 1997; Smalt et al., 1997; You et al., 2000). However, as protrusions are shown to alter the predicted mechanical environment, a major implication of this study is that physiologic subcellular geometries can possibly bridge the gap between *in vitro* and *in vivo* models (where up to an order of magnitude difference has been predicted in the past) and lead to the elucidation of the cellular mechanisms of bone adaptation.

Conflict of interest

All authors have no conflict of interest.

Acknowledgments

The authors would like to thank Dr. Gautschi of University of Zurich for acquiring the electron micrographs used in this manuscript. This study was supported by The Whitaker Foundation (RG-02-0527). This investigation was conducted in a facility constructed with support from Research Facilities Improvement Program Grant Number C06 RR12463-01 from the National Center for Research Resources, National Institutes of Health.

References

- Almekinders, L.C., Banes, A.J., Ballenger, C.A., 1993. Effects of repetitive motion on human fibroblasts. *Medicine and Science in Sports and Exercise* 25, 603–607.
- Anderson, E.J., Knothe Tate, M.L., 2007. Open access to novel dual flow chamber technology for *in vitro* cell mechanotransduction, toxicity and pharmacokinetic studies. *Biomedical Engineering Online* 6, 46.
- Anderson, E.J., Kaliyamoorthy, S., Alexander, J.I.D., Knothe Tate, M.L., 2005. Nano-microscale models of periosteocytic flow show differences in stresses imparted to cell body and processes. *Annals of Biomedical Engineering* 33, 52–62.
- Anderson, E.J., Falls, T.D., Sorkin, A.M., Knothe Tate, M.L., 2006. The imperative for controlled mechanical stresses in unraveling cellular mechanisms of mechanotransduction. *Biomedical Engineering Online* 5, 27.
- Anderson, E.J., Kreuzer, S., Small, O., Knothe Tate, M.L., 2008. Pairing computational and scaled physical models to determine permeability as a measure of cellular communication in micro-and nano-scale pericellular spaces. *Microfluidics and Nanofluidics* 4, 193–204.
- Burger, E.H., Veldhuijzen, J.P., 1993. Influence of mechanical factors on bone formation, resorption and growth *in vitro*. In: Hall, B.K. (Ed.), *Bone*, vol. 7. CRC Press, Boca Raton, FL, USA, pp. 37–56.
- Donahue, S.W., Donahue, H.J., Jacobs, C.R., 2003. Osteoblastic cells have refractory periods for fluid-flow-induced intracellular calcium oscillations for short bouts of flow and display multiple low-magnitude oscillations during long-term flow. *Journal of Biomechanics* 36, 35–43.
- Fritton, S.P., McLeod, K.J., Rubin, C.T., 2000. Quantifying the strain history of bone: spatial uniformity and self-similarity of low-magnitude strains. *Journal of Biomechanics* 33, 317–325.
- Frost, H.M., 1987. Bone “mass” and the “mechanostat”: a proposal. *Anatomical Record* 219, 1–9.
- Goodship, A.E., Lanyon, L.E., McFie, H., 1979. Functional adaptation of bone to increased stress. An experimental study. *Journal of Bone and Joint Surgery American* 61, 539–546.
- Guilak, F., Ratcliffe, A., Mow, V.C., 1995. Chondrocyte deformation and local tissue strain in articular cartilage: a confocal microscopy study. *Journal of Orthopaedic Research* 13, 410–421.
- Han, Y., Cowin, S.C., Schaffler, M.B., Weinbaum, S., 2004. Mechanotransduction and strain amplification in osteocyte cell processes. *Proceedings of the National Academy of Science* 101, 16689–16694.
- Jacobs, C.R., Yellowley, C.E., Davis, B.R., Zhou, Z., Cimbal, J.M., Donahue, H.J., 1998. Differential effect of steady versus oscillating flow on bone cells. *Journal of Biomechanics* 31, 969–976.
- Klein-Nulend, J., van der Plas, A., Semeins, C.M., Ajubi, N.E., Frangos, J.A., Nijweide, P.J., Burger, E.H., 1995. Sensitivity of osteocytes to biomechanical stress *in vitro*. *Federation of American Societies for Experimental Biology* 9, 441–445.
- Knapp, H.F., Reilly, G.C., Stemmer, A., Niederer, P., Knothe Tate, M.L., 2002. Development of preparation methods for and insights obtained from atomic force microscopy of fluid spaces in cortical bone. *Scanning* 24, 25–33.
- Knothe Tate, M.L., 2001a. Mixing mechanisms and net solute transport in bone. *Annals of Biomedical Engineering* 29, 810–811.
- Knothe Tate, M.L., 2001b. Interstitial fluid flow. In: Cowin, S.C. (Ed.), *Bone Biomechanics Handbook*, second ed. CRC Press, New York, NY, USA, pp. 1–29.
- Knothe Tate, M.L., 2003. “Whither flows the fluid in bone?” An osteocyte’s perspective. *Journal of Biomechanics* 36, 1409–1424.
- Knothe Tate, M.L., Knothe, U., Niederer, P., 1998a. Experimental elucidation of mechanical load-induced fluid flow and its potential role in bone metabolism and functional adaptation. *American Journal of Medical Sciences* 316, 189–195.
- Knothe Tate, M.L., Niederer, P., Knothe, U., 1998b. *In vivo* tracer transport through the lacunocanalicular system of rat bone in an environment devoid of mechanical loading. *Bone* 22, 107–117.
- Knothe Tate M.L., Niederer P., 1998. A theoretical FE-based model developed to predict the relative contribution of convective and diffusive transport mechanisms for the maintenance of local equilibria within cortical bone. *Advances in Heat and Mass Transfer in Biotechnology*, (Ed. S. Clegg) The American Society of Mechanical Engineers, HTD - Vol. 362/BED - Vol. 40, 133–142.
- McGarry, J.G., Klein-Nulend, J., Mullender, M.G., Prendergast, P.J., 2005. A comparison of strain and fluid shear stress in stimulating bone cell responses—a computational and experimental study. *Federations of American Societies for Experimental Biology* 19, 482–484.
- Nicolella, D.P., Moravits, D.E., Gale, A.M., Bonewald, L.F., Lankford, J., 2006. Osteocyte lacunae tissue strain in cortical bone. *Journal of Biomechanics* 39, 1735–1743.
- Owan, I., Burr, D.B., Turner, C.H., Qiu, J., Tu, Y., Onyia, J.E., Duncan, R.L., 1997. Mechanotransduction in bone: osteoblasts are more responsive to fluid forces than mechanical strain. *American Journal of Physiology* 273, C810–C815.
- Pienkowski, D., Pollack, S.R., 1983. The origin of stress-generated potentials in fluid-saturated bone. *Journal of Orthopaedic Research* 1, 30–41.
- Reich, K.M., Frangos, J.A., 1991. Effect of flow on prostaglandin E2 and inositol trisphosphate levels in osteoblasts. *American Journal of Physiology* 261, C428–C432.
- Reilly, G.C., Knapp, H.F., Stemmer, A., Neiderer, P., Knothe Tate, M.L., 2001. Investigation of the morphology of the lacunocanalicular system of cortical bone using atomic force microscopy. *Annals of Biomedical Engineering* 29, 1074–1081.
- Rubin, C.T., Lanyon, L.E., 1984. Regulation of bone formation by applied dynamic loads. *Journal of Bone and Joint Surgery American* 66, 397–402.
- Scherft, J.P., 1972. The *lamina limitans* of the organic matrix of calcified cartilage and bone. *Journal of Ultrastructural Research* 38, 318–331.
- Smalt, R., Mitchell, F.T., Howard, R.L., Chambers, T.J., 1997. Induction of NO and prostaglandin E2 in osteoblasts by wall-shear stress but no mechanical strain. *American Journal of Physiology* 273, E751–E758.
- Steck, R., Knothe Tate, M.L., 2005. *In silico* stochastic network models that emulate the molecular sieving characteristics of bone. *Annals of Biomedical Engineering* 33, 87–94.
- Tami, A.E., Nasser, P., Verborgt, O., Schaffler, M.B., Knothe Tate, M.L., 2002. The role of interstitial fluid flow in the remodeling response to fatigue loading. *Journal of Bone and Mineral Research* 7, 2030–2037.
- Verborgt, O., Gibson, G.J., Schaffler, M.B., 2000. Loss of osteocyte integrity in association with microdamage and bone remodeling after fatigue *in vivo*. *Journal of Bone and Mineral Research* 15, 60–67.
- Weinbaum, S., Cowin, S.C., Zeng, Y., 1994. A model for the excitation of osteocytes by mechanical loading-induced bone fluid shear stresses. *Journal of Biomechanics* 27, 339–360.

- You, J., Yellowley, C.E., Donahue, H.J., Zhang, Y., Chen, Q., Jacobs, C.R., 2000. Substrate deformation levels associated with routine physical activity are less stimulatory to bone cells relative to loading-induced oscillatory fluid flow. *Journal of Biomechanical Engineering* 122, 387–393.
- You, L., Cowin, S.C., Schaffler, M.B., Weinbaum, S., 2001. A model for strain amplification in the actin cytoskeleton of osteocytes due to fluid drag on pericellular matrix. *Journal of Biomechanics* 34, 1375–1386.
- You, L.D., Weinbaum, S., Cowin, S.C., Schaffler, M.B., 2004. Ultrastructure of the osteocyte process and its pericellular matrix. *Anatomical Record* 278, 505–513.